

Article

NO_x Removal by Selective Catalytic Reduction with Ammonia over a Hydrotalcite-Derived NiFe Mixed Oxide

Ruonan Wang ¹, Xu Wu ^{1,*}, Chunlei Zou ¹, Xiaojian Li ¹ and Yali Du ^{2,*}

¹ College of chemistry and Chemical Engineering, Taiyuan University of Technology, Taiyuan 030024, China; wangruonan0490@link.tyut.edu.cn (R.W.); zouchunlei0492@link.tyut.edu.cn (C.Z.); mlxiaojian@163.com (X.L.)

² College of Chemistry and Chemical Engineering, Jinzhong University, Jinzhong 030619, China

* Correspondence: wuxu@tyut.edu.cn (X.W.); dy10037@163.com (Y.D.);
Tel.: +86-035-1601-8528 (X.W.); +86-13513635848 (Y.D.)

Received: 24 July 2018; Accepted: 6 September 2018; Published: 8 September 2018



Abstract: A series of NiFe mixed oxide catalysts were prepared via calcining hydrotalcite-like precursors for the selective catalytic reduction of nitrogen oxides (NO_x) with NH₃ (NH₃-SCR). Multiple characterizations revealed that catalytic performance was highly dependent on the phase composition, which was vulnerable to the calcination temperature. The MO_x phase (M = Ni or Fe) formed at a lower calcination temperature would induce more favorable contents of Fe²⁺ and Ni³⁺ and as a result contribute to the better redox capacity and low-temperature activity. In comparison, NiFe₂O₄ phase emerged at a higher calcination temperature, which was expected to generate more Fe species on the surface and lead to a stable structure, better high-temperature activity, preferable SO₂ resistance, and catalytic stability. The optimum NiFe-500 catalyst incorporated the above virtues and afforded excellent denitration (DeNO_x) activity (over 85% NO_x conversion with nearly 98% N₂ selectivity in the region of 210–360 °C), superior SO₂ resistance, and catalytic stability.

Keywords: NiFe-LDH; mixed oxide; NiFe₂O₄ spinel; NO_x; NH₃-SCR

1. Introduction

Emission of nitrogen oxides (NO_x) is a main contributing factor to the induction of regional air pollution and ecosystem acidification [1]. During the past few decades, stringent regulations on NO_x emissions have been issued worldwide and various measures have been devoted to diminish NO_x, among which the removal of NO_x from stationary sources by selective catalytic reduction of NO_x with NH₃ (NH₃-SCR) has been attracting significant attention due to the low cost and high efficiency [2–4]. The most adopted SCR catalysts in practical applications are V-based catalysts, while the toxicity of active vanadium species, together with high N₂O formation at high temperatures, restricts their further application [5]. Therefore, for the current situation, developing environmentally friendly substitutive catalysts with excellent efficiency, strong stability, and high SO₂ resistance in NH₃-SCR is imperative.

Recently, great efforts have been made to exploit novel NH₃-SCR catalysts, and some transition metal oxide catalysts have received wide attention [6–8]. Notably, iron-based catalysts have been considered as a potential candidate for the NH₃-SCR application due to their high reactivity, cost-effectiveness, superior SO₂ durability, and non-toxicity. However, pure iron catalysts are subject to the limitations of a low acid amount [9] and inferior N₂ selectivity beyond 330 °C [10,11].

Up to now, a lot of reports have found that introducing other active ingredients (e.g., titanium oxides [12], manganese oxides [13], or tungsten oxides [2]) is an effective way to promote the denitration (DeNO_x) performance of iron-based catalysts. Especially, nickel species possess abundant surface

acidity sites [14] and a favorable ability to increase the N_2 selectivity of NH_3 -SCR reactions [15,16], which was expected to be introduced into the iron-based catalytic system [17]. Furthermore, nickel oxides are considered as valuable materials to induce a synergistic effect with other active species, such as $NiMnO_x$ [18,19] and $NiTiO_x$ [20], which are very sensitive to the synthesis process.

It was reported that layered double hydroxide (LDHs) materials are excellent precursors for the preparation of metal oxide catalysts with the desired chemical and phase composition [21]. Thermal decomposition of hydrotalcite-like materials could produce layered double oxides (LDOs) possessing a relatively high surface area, which could promote the catalytic performance.

Herein, a series of economical and eco-friendly NiFe mixed oxides catalysts were prepared via calcining a hydrotalcite-like compound at various temperatures. The NH_3 -SCR activity, SO_2 resistance, and stability were evaluated for the different NiFe mixed oxides catalysts. The correlations among phase composition, structure, and catalytic performance were systematically explored by XRD (X-ray diffraction), FT-IR (Fourier Transform Infrared), TG (thermogravimetric analysis), N_2 physisorption, NH_3 -TPD (NH_3 -Temperature Programmed Desorption), H_2 -TPR (H_2 -Temperature Programmed Reduction), and XPS (X-ray Photoelectron Spectroscopy). It was proved that the $DeNO_x$ performance was highly dependent on the phase composition of NiFe mixed oxides catalysts, which was available via adjusting the calcination temperature of NiFe-LDH. This work may serve as an important reference for LDH precursors to be tailored for potential applications in adjusting the phase component and catalytic performance.

2. Results and Discussion

NH_3 -SCR reactions over NiFe mixed oxides catalysts at various calcination temperatures (400 °C, 500 °C, and 600 °C) were performed during 150–450 °C and the results are given in Figure 1A. It is clear that the NiFe-400 sample showed rather low NH_3 -SCR efficiency with an obviously narrow operation temperature window. The $DeNO_x$ activity and temperature window for the NiFe-500 and NiFe-600 samples were promoted dramatically in comparison to that of the NiFe-400 catalyst. The NiFe-600 catalyst exhibited lower NO_x conversion than the NiFe-500 catalyst at temperatures below 330 °C, while it behaved better in the higher temperature region, which implied that the higher calcination temperature was conducive to high-temperature SCR activity. As demonstrated in Figure 1B, all NiFe mixed oxides catalysts afforded superior N_2 selectivity: nearly 98% below 360 °C. When temperatures exceeded 360 °C, the N_2 selectivity of the NiFe-500 and NiFe-600 samples showed a slight decline compared with the NiFe-400 catalyst. Obviously, the NiFe-500 catalyst was the most promising candidate for NH_3 -SCR, affording above 85% $DeNO_x$ activity within the widest temperature region of 210–360 °C and superior N_2 selectivity over the whole tested temperature range.

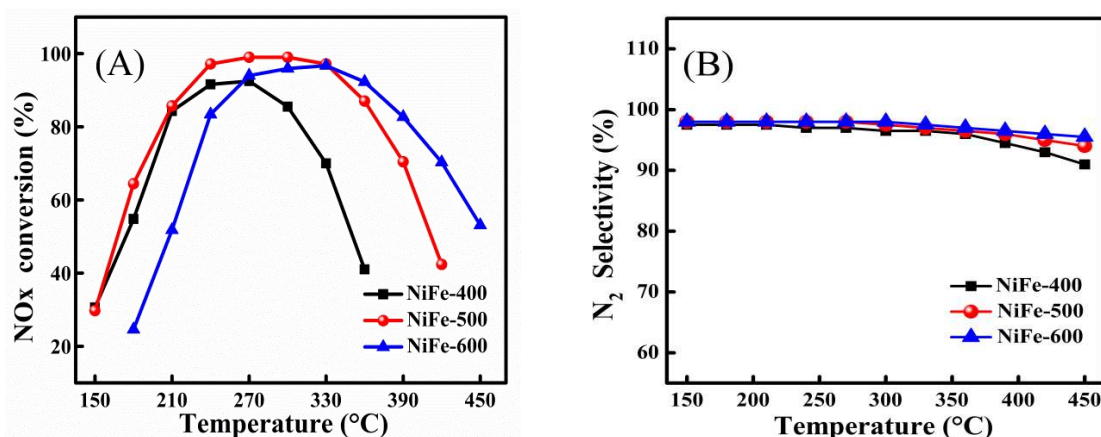


Figure 1. Cont.

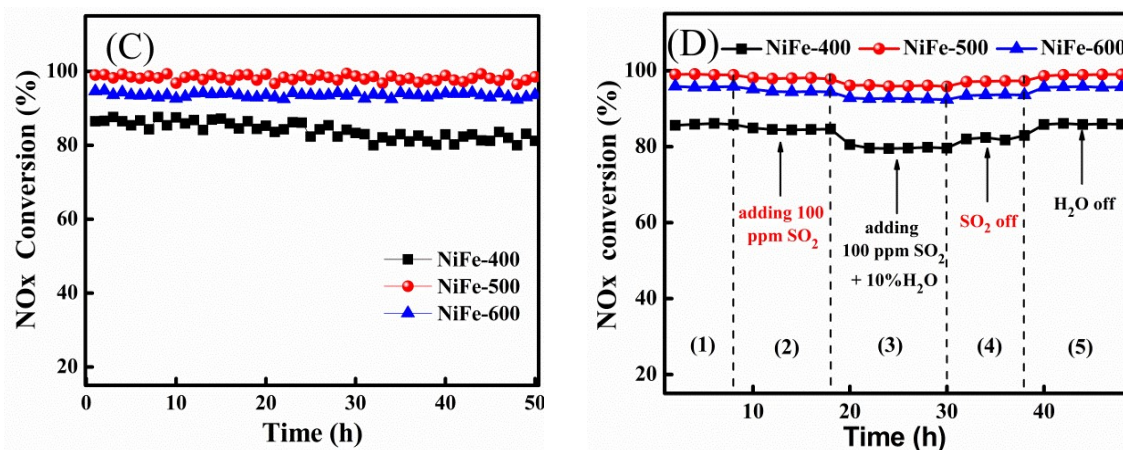


Figure 1. Catalytic performance of the serial NiFe-layered double oxide (LDO) catalysts: (A) nitrogen oxide (NO_x) conversion; (B) N₂ selectivity; (C) stability tests at 300 °C; (D) SO₂/H₂O resistance tests at 300 °C. Reaction conditions: 600 ppm NO, 600 ppm NH₃, 5% O₂, 100 ppm SO₂ (when used), 10% H₂O (when used), balance N₂, gas hourly space velocity (GHSV) = 45,000 h⁻¹.

The stability is an important indicator to estimate the properties of catalysts. The stability tests were performed at 300 °C for 50 h over each catalyst under the reaction conditions of 600 ppm NO, 600 ppm NH₃, 5.0% O₂, and balanced with N₂. As presented in Figure 1C, the DeNO_x activity of the NiFe-500 and NiFe-600 catalysts slightly fluctuated with only ±1% variance, indicating fine stability. Comparatively, the NiFe-400 sample displayed the relatively worst stability. Such different stabilities can be ascribed to the different stabilities of the mixed oxides' structures. Thus, the NiFe-500 and NiFe-600 catalysts possessed a more stable structure in comparison with the NiFe-400 catalyst.

The presence of H₂O and SO₂ in the actual exhaust usually inhibits the NH₃-SCR of NO_x [22]. Therefore, it is of great importance to evaluate the H₂O and/or SO₂ tolerance under the reaction conditions. The H₂O and/or SO₂ tolerance of the serial NiFe mixed oxides catalysts was investigated at 300 °C under the reaction conditions of 600 ppm NO, 600 ppm NH₃, 5% O₂, 0 or 100 ppm SO₂, 0 or 10.0% H₂O, and balanced with N₂. As depicted in Figure 1D, at the first stage, the NO_x conversion for the NiFe-400, NiFe-500, and NiFe-600 catalysts was maintained at around 85%, 99%, and 96%, respectively. After adding 100 ppm SO₂ into the reaction gas, the NO_x conversion decreased slightly. However, the co-existence of 100 ppm SO₂ and 10% H₂O led to a gradual decrease to some extent in NO_x conversion, where the decrease was only about 2% for the NiFe-500 and NiFe-600 samples while around a 5% decrease was displayed for NiFe-400. After purging off SO₂ and H₂O, the NO_x conversion gradually recovered to the original values. Thus, the NiFe-500 and NiFe-600 catalysts possessed an excellent SO₂ and H₂O resistance ability in comparison to the NiFe-400 catalyst.

XRD is an essential technology to evaluate the structure of catalysts. The XRD pattern of the NiFe-LDH precursor is presented in Figure 2A. The characteristic reflections at 2θ values of 11.7°, 23.2°, 34.5°, 39.1°, 45.6°, and 59.8° can be observed, which were correspondingly indexed to the (003), (006), (012), (015), (018), and (110) planes according to the standard card (JCPDS no.15-0087). The absence of other crystalline phases hinted at the successful fabrication of NiFe-LDHs with high purity.

The FT-IR spectrum of NiFe-LDH is illustrated in Figure 2B. An intense and board peak at 3429 cm⁻¹ corresponded to the stretching vibration of the -OH group in the NiFe brucite-like layers, the interlayer water molecules, and the lattice water [23]. The peak that occurred at 2987 cm⁻¹ can be assigned to a CO₂-H₂O bridging bond [24]. The vibration of the angular deformation of H₂O molecules was observed at 1601 cm⁻¹ [23]. The peaks at 1385 cm⁻¹ belonged to the stretching vibrations of carbonate ions [25]. Additionally, the peak located at 676 cm⁻¹ might be correlated to the vibration of M-O (Fe-O, Fe-O-Ni or Ni-O) on the layer of the NiFe-LDH samples [26]. Both XRD and FT-IR data confirmed that NiFe-LDH was prepared successfully with CO₃²⁻ as an interlayer anion.

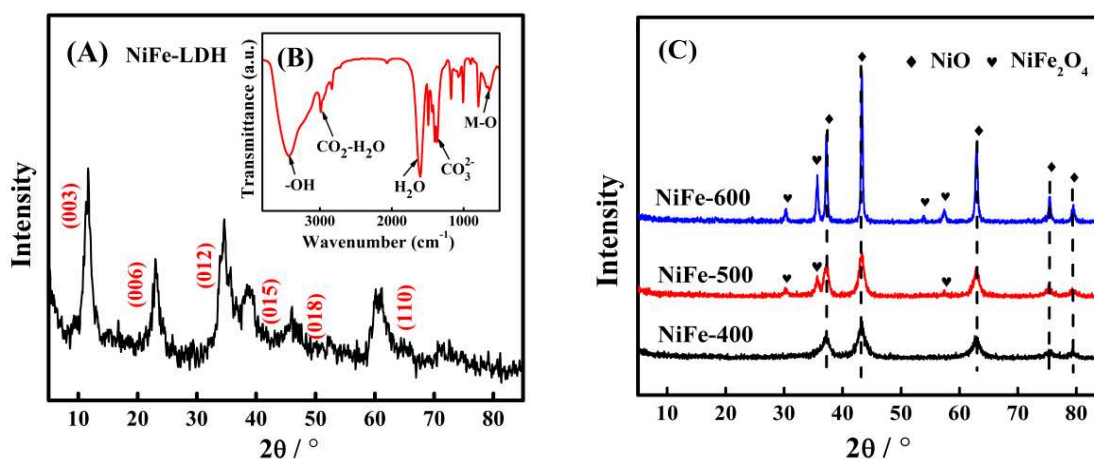


Figure 2. XRD pattern (A) and FT-IR spectrum (B) of NiFe- layered double hydroxide (LDH) precursor; XRD patterns of NiFe-LDO catalysts (C).

The process of thermal decomposition of the NiFe-LDH precursor into mixed oxides was studied by TG coupled with MS (mass spectrometer) analysis (TG-MS). From the TG and DTG (derivative thermogravimetry) curves in Figure 3A, three major weight-loss stages were observed visually. The initial reduction in mass occurred between 80 °C and 180 °C (approximately 9 wt.%) and arose from the desorption of the surface adsorbed and interlayer water and CO_2 molecules. The second mass loss stage occurred at the temperature range of 190–350 °C (about 13 wt.%) and mainly released H_2O , CO_2 , and NO_2 , which were detected by online MS analysis (Figure 3B). This rapid and major mass loss can be assigned to the dehydroxylation of the inorganic layers and decomposition of interlayer anions (NO_3^- and CO_3^{2-}) [27] accompanied by the collapse of the hydrotalcite structure. A small DTG exothermic peak at about 395 °C observed in the Figure 3A corresponds to the release of CO_2 and NO_2 in the MS curves, which was attributed to the degradation of nitrates and carbonates with high thermal stability. Based on the above, stable NiFe mixed oxides catalysts can be obtained when hydrotalcite-like precursors are calcined at over 400 °C.

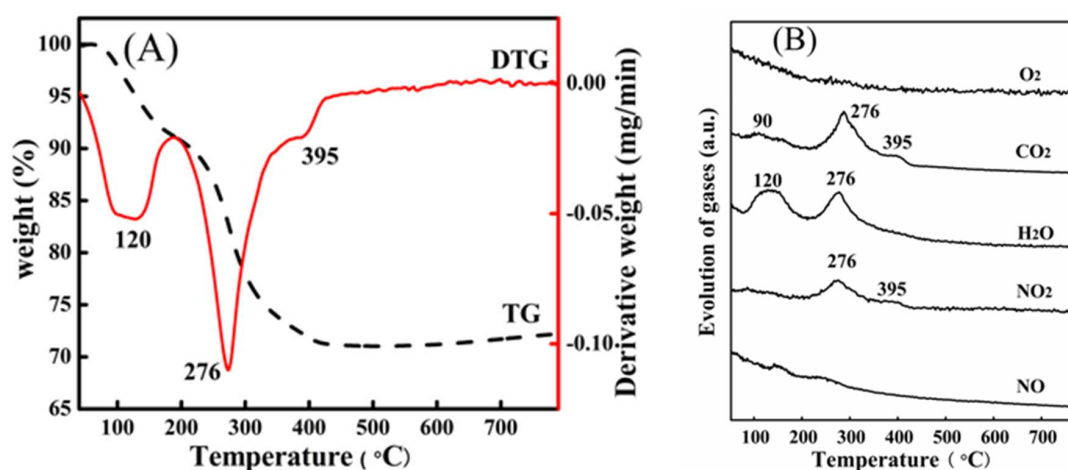


Figure 3. Results of TG and DTG studies (A) combined with MS analysis (B) for the NiFe-LDH sample.

An XRD analysis was performed for the serial NiFe mixed oxides catalysts, which were produced by calcining NiFe-LDH at different temperatures (400–600 °C). As exhibited in Figure 2C, the calcination temperature was an important factor affecting the formation of crystalline phase. As the calcination temperature increases from 400 °C to 600 °C, the diffraction peaks were found to significantly sharpen, representing the mushrooming of crystallinity and particle size. Meanwhile, new crystal phases progressively appeared. For the NiFe-400 sample, all diffraction peaks at 37.0° , 43.3° , 63.2° , 75.7° ,

and 78.8° could be assigned to NiO phase (PDF # 44-1159). The absence of diffraction peaks of Fe species, existing in the form of oxides (e.g., FeO, Fe₂O₃, and Fe₃O₄), manifested their high dispersion or presence in the crystal lattice of NiO. The indicative diffraction peaks of NiFe₂O₄ spinel were emergent in NiFe-500 and markedly enhanced for the NiFe-600 sample, which were located at 2θ values of 30.4° , 35.6° , 53.8° , and 57.5° (PDF # 10-0325). Notably, according to the literature [28], a NiFe₂O₄ spinel possesses an inverse structure and can be written as Fe[NiFe]O₄, in which half of the Fe³⁺ occupies the tetrahedral sites with the octahedral sites comprised of a 1:1 ratio of Ni²⁺ and Fe³⁺ cations. It was reported that such an inverse NiFe₂O₄ spinel is a valuable material with structural stability and the possibility for bifunctional redox properties [28,29]. Combining the results in the catalytic performance tests, the NiFe₂O₄ spinel could be confirmed to be the expected phase in this system.

The nitrogen adsorption and desorption isotherms of NiFe mixed oxides catalysts are displayed in Figure 4A, in which can clearly be observed the typical shape of type IV isotherms curves (IUPAC classification), indicating the presence of 2–50 nm mesopores [30,31]. The NiFe-400 and NiFe-500 samples displayed a typical type H2 hysteresis loop that verified the existence of an “ink bottle” state structure, whereas the NiFe-600 catalyst presented the narrow type H3 hysteresis loop, demonstrating the existence of a “slit”-shaped mesopore [9,32]. Meanwhile, the pore diameter distribution of the serial catalysts can be visually observed from Figure 4B, where NiFe-500 exhibited the more intensive distribution in the region of 1–6 nm. The Brunauer–Emmett–Teller (BET) surface area and the average pore diameter of the as-prepared catalysts are listed in Table 1. The BET specific surface areas calculated by N₂ desorption isotherms were clearly seen to drop sharply with the increase of the calcination temperature in Table 1. However, the order of the catalysts by average pore diameter was NiFe-600 (15.5 nm) > NiFe-400 (5.1 nm) > NiFe-500 (4.0 nm). As discussed in the XRD analysis, with the increasing of calcination temperature, the crystallinity and particle size were both increased. Thus, the BET surface areas were decreased, which is in agreement with the literature [33]. In addition, in comparison to NiFe-400, NiFe-500 showed a smaller pore diameter, which may be due to the shrinkage of pores accompanied by the increase in crystallinity. However, for NiFe-600, a high crystallinity NiFe₂O₄ spinel was formed, which may result in the formation of a “stacked hole” with a larger pore diameter. The relatively larger specific surface area and even porous structures can provide more catalytic centers, which might account for the better DeNO_x performance.

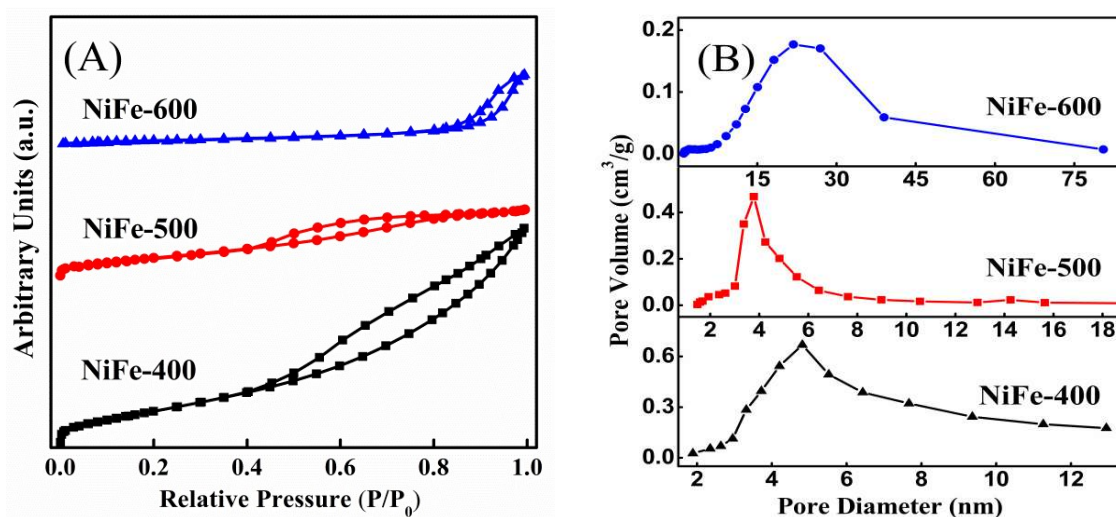


Figure 4. N₂ adsorption and desorption isotherms (A) and pore diameter distribution (B) of the serial NiFe-LDO catalysts.

The surface acidity and acid strength distribution of the NiFe mixed oxides catalysts were investigated by NH₃-TPD experiments. As illustrated in Figure 5A, the NH₃-TPD curves showed two ammonia desorption peaks for each sample in the 70–700 °C range. The first desorption peak

centered at around 120 °C corresponds to the physisorbed NH₃ or weakly acidic sites [34]. The other peak located at around 480 °C can be assigned to the chemical adsorbed ammonia on strong Lewis and Brønsted acidity sites [35]. The amount of total NH₃ adsorption and the proportion for every type of acid site were calculated from the integrated areas of the corresponding peaks. The calculation results were normalized and are listed in Table 2. It is clear that the increase of calcination temperature resulted in a dramatic reduction of ammonia adsorption and surface acidity. The desorption amount of NiFe-500 and NiFe-600 decreased by 35% and 73%, respectively. In addition, with the calcination temperature increasing from 400 °C to 600 °C, the proportion of weakly acidic sites shows an obvious rise from 34.5% to 52.4%, while the proportion of the strongly acidic sites decreased from 65.5% to 47.6%. Combined with the results of XRD and BET, we speculated that the increase of calcination temperature resulted in severe agglomeration of iron species and the acid center was covered in this process. More acid sites should be conducive to promote DeNO_x activity. However, the NiFe-400 catalyst afforded the worst NH₃-SCR performance though it owned the maximum acid quantity, suggesting that the number of acid sites was not the only factor to affect catalytic performance. Moreover, to our great interest, the NiFe-600 catalyst possessed the lowest number acid sites, but its high-temperature DeNO_x activity was satisfactory. The DeNO_x mechanism was further analyzed as below. It was confirmed that an iron-based mixed oxide catalyst would follow the Langmuir–Hinshelwood mechanism under 250 °C, where both NH₃ and NO would be adsorbed to all of the acid sites and then transformed to the corresponding intermediate [36]. The dramatic decrease of acid quantity for NiFe-600 resulted in the absence of adsorption of the reactant; accordingly, the low-temperature activity decreased. At medium and higher temperatures, the catalyst would fit the Eley–Rideal mechanism [31,37], where only the adsorption and activation process of NH₃ was conducted, generating the reaction between the adsorbed intermediate and gaseous-state NO. Therefore, the residual acid sites were still enough to absorb the majority of the NH₃ despite the evident decrease.

Table 1. Brunauer–Emmett–Teller (BET) surface areas and average pore diameter of the samples.

Catalysts	BET Surfaces Areas (m ² /g)	Average Pore Diameter (nm)
NiFe-400	169.3	5.1
NiFe-500	89.6	4.0
NiFe-600	20.9	15.5

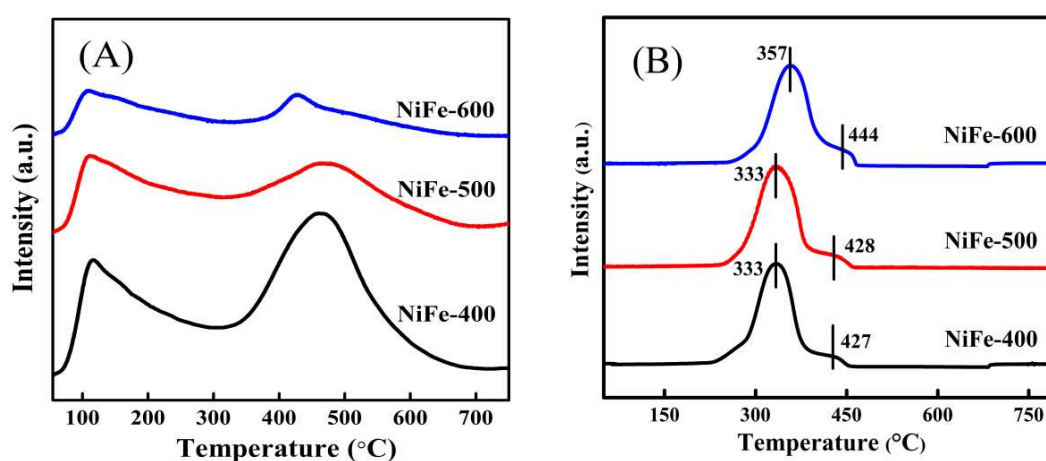


Figure 5. NH₃-TPD profiles (A) and H₂-TPR patterns (B) of the serial NiFe catalysts.

The H₂-TPR technique was employed to determine the reducibility of the as-prepared NiFe mixed oxides catalysts. Over all samples, two noticeable reduction peaks are exhibited in Figure 5B. According to the literature [38,39], the reduction peak located at the lower temperature region (200–400 °C) may be assigned to the reduction of Ni²⁺ (Ni³⁺) to Ni⁰ (Peak 1), and the reduction peak at the higher

temperature region (400–450 °C) could represent the reduction of Fe species (Peak 2). However, it was reported that the reduction peaks of mixed oxides usually do not correspond to only one kind of metal oxide [40]. Hence, the theoretical (denoted as E) and actual (denoted as A) H₂ consumption of each catalyst were calculated and are shown in Table 3. For all samples, the amount of total theoretical H₂ consumption was higher than that of the total actual H₂ consumption, implying the existence of an incomplete reduction of active species. Therein, the actual H₂ consumption amount of Ni species (peak 1) was higher than the theoretical values for each catalyst ($A_1 > E_1$), while Fe species (peak 2) were the opposite ($A_2 < E_2$). Therefore, the first reduction peak may be ascribed to the co-reduction of Ni as well as partial Fe species and the second peak may be only attributed to the Fe species. From Table 3, it was also clear that the NiFe-400 and NiFe-500 catalysts exhibited a similar position of reduction peaks and the NiFe-600 catalyst significantly shifted to high-temperature zones, presenting the worst reducibility for NiFe-600, which can well-explain its degraded DeNO_x activity at a low temperature compared with the NiFe-400 and NiFe-500 catalysts.

Table 2. Amount and proportion of NH₃ desorption of the serial catalysts.

Catalysts	Total Amount of NH ₃ Desorption ^a	Proportion of NH ₃ Desorption (%)	
		Weak Acid Sites (55–300 °C)	Strong Acid Sites (300–700 °C)
NiFe-400	1	34.5	65.5
NiFe-500	0.65	42.5	57.5
NiFe-600	0.27	52.4	47.6

^a Normalized by the NH₃ desorption peaks area of the NiFe-400 sample (28,487.8 a.u.).

Table 3. The reduction peaks temperature (°C) and H₂ consumption (mmol g⁻¹) of each catalyst.

Catalysts	Peak 1			Peak 2			Total Actual H ₂ Consumption	Total Theoretical H ₂ Consumption
	T ₁	A ₁	E ₁	T ₂	A ₂	E ₂		
NiFe-400	333	13.99	13.86	427	0.59	0.77	14.58	14.63
NiFe-500	333	14.21	14.05	428	0.41	0.88	14.62	14.93
NiFe-600	357	13.68	12.10	444	0.95	2.62	14.63	14.72

where T₁ and T₂ refer to the reduction peak temperature; A₁ and A₂ refer to the actual H₂ consumption of peak 1 and peak 2, respectively; and E₁ and E₂ refer to the theoretical H₂ consumption of peak 1 and peak 2, respectively.

XPS analysis was performed to determine the surface components and valence states of elements presented on the catalyst surfaces. The XPS spectra of Fe 2p and Ni 2p_{3/2} are shown in Figure 6 and the corresponding surface atomic concentrations as well as the proportion of different valence states are listed in Table 4.

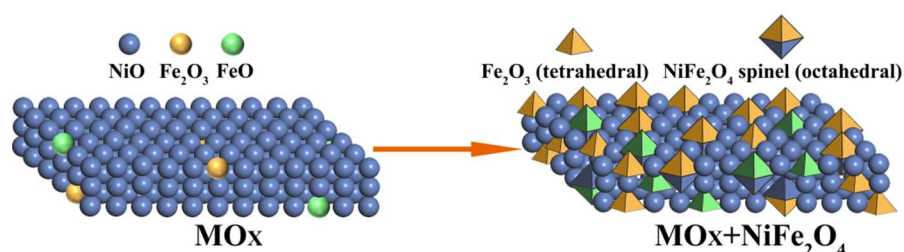


Figure 6. The ideal model of catalysts with MO_x (M = Ni or Fe) or multiple phases (MO_x and a NiFe₂O₄ spinel).

According to Table 4, the amounts of surface Fe species showed a monotonic increase for the NiFe-400, NiFe-500, and NiFe-600 catalysts. As discussed in the XRD analysis section, when NiFe-LDH was calcined at 400 °C, iron species existed in the form of FeO_x, which should be mostly covered by Ni

species. With the increment of calcination temperature, NiFe₂O₄ spinels were generated. Fe species were gradually exposed or transferred to the surface of the catalysts, and the ideal model is displayed in Figure 6. It is well-known that more Fe species could result in better high-temperature activity; thus, DeNO_x activity at high temperatures (>330 °C) displaying the order of NiFe-600 > NiFe-500 > NiFe-400 can be reasonable.

Table 4. Surface atomic concentration and oxidation states.

Catalysts	Fe 2p		Ni 2p	
	Fe (%)	Fe ³⁺ / (Fe ²⁺ + Fe ³⁺) (%)	Ni (%)	Ni ³⁺ / (Ni ²⁺ + Ni ³⁺) (%)
NiFe-400	1.7	51.4	28.3	72.5
NiFe-500	2.2	43.8	30.9	75.5
NiFe-600	5.4	66.5	25.6	60.1

For the XPS spectra of Fe 2p in Figure 7A, two main peaks assigned to Fe 2p_{3/2} and Fe 2p_{1/2} can be observed centered at a binding energy of approximately 711 eV and 724 eV, respectively. By performing peak-fitting deconvolution, the Fe 2p_{3/2} spectra were fitted into sub-bands located at approximately 710.9 eV and 712.7 eV, which corresponded to Fe²⁺ and Fe³⁺, respectively [41]. As shown in Figure 7B, the Ni 2p_{3/2} spectra can be separated into three characteristic peaks at 854.1, 855.9, and 861.4 eV, which can be ascribed to the Ni²⁺, Ni³⁺, and satellite peaks, respectively [42]. Combined with the data in Table 2, it was clear that the Ni³⁺ content on the surface of the NiFe-500 sample (75.5%) was higher than that of the NiFe-400 sample (72.5%), but the content of the surface Fe³⁺ species was opposite for the two catalysts, which indicated that increasing the calcination temperature could result in a redox reaction between Ni²⁺ and Fe³⁺ to form Ni³⁺ and Fe²⁺ (Ni²⁺ + Fe³⁺ ⇌ Ni³⁺ + Fe²⁺). However, the amount of surface Ni³⁺ decreased to 60.1% with the increase in calcination temperature from 500 °C to 600 °C for the NiFe catalyst, which can be attributed to the formation of more high-crystallinity NiFe₂O₄ spinels, so it was difficult for the reaction (Ni²⁺ + Fe³⁺ ⇌ Ni³⁺ + Fe²⁺) to occur on the surface of the catalyst. Thus, comparatively, the redox reaction (Ni²⁺ + Fe³⁺ ⇌ Ni³⁺ + Fe²⁺) may more easily occur for the NiFe-500 sample. Such interaction in the bimetallic oxide was similar to that previously reported [30,43] and it was considered to be favorable for the creation of a redox cycle and further promoted the catalytic activity, especially at low temperatures.

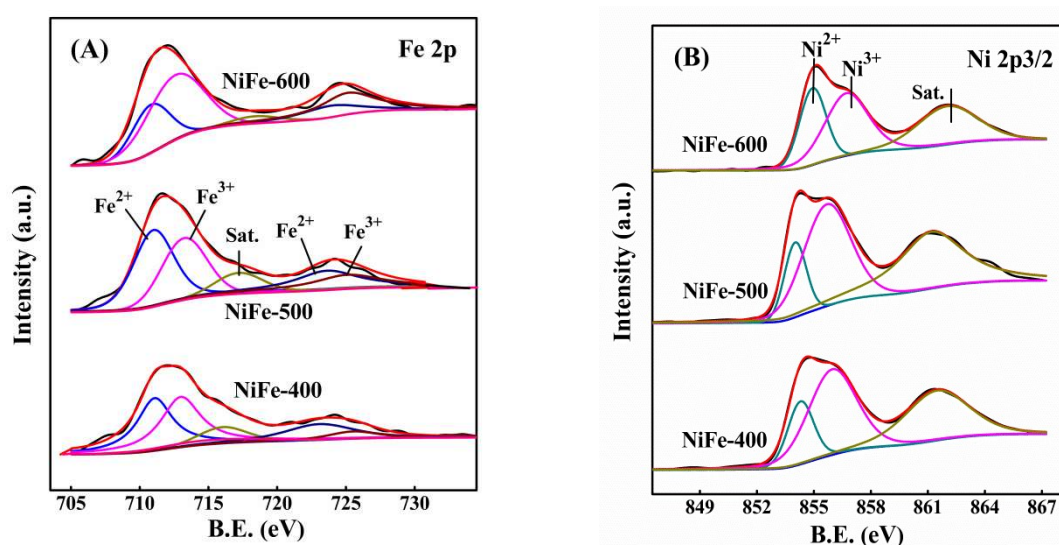


Figure 7. XPS spectra of the serial catalysts: (A) Fe 2p and (B) Ni 2p.

3. Materials and Methods

3.1. Catalyst Preparation

The NiFe hydrotalcite-like precursor with the molar ratio of Ni to Fe being 4 was prepared by the urea hydrolysis method [44]. First, a urea solution and a mixed solution with $\text{Ni}(\text{NO}_3)_2 \cdot 6\text{H}_2\text{O}$, $\text{Fe}(\text{NO}_3)_3 \cdot 9\text{H}_2\text{O}$, and sodium citrate in the corresponding ratio were dissolved fully with deionized water. Afterwards, the solution was transferred to a beaker and hydrothermally treated at 120 °C for 24 h. The NiFe-LDH precursors were obtained after extraction, filtration, washing, and drying at 60 °C for 12 h. Subsequently, the precursors were calcined at the required temperature (400–600 °C) for 5 h to obtain the NiFe mixed oxides. Finally, the NiFe catalysts were crushed and sieved through 40–60 mesh for catalytic evaluation.

3.2. Catalyst Characterization

XRD patterns of the samples were characterized using a DX-2700 instrument (Dandong Aolong Radiative Instrument Group Co. Ltd, Liaoning, China) with a Cu K α radiation source ($\lambda = 1.54184 \text{ \AA}$, 40 KV, and 30 mA) in the 2θ range of 5–85° at a step of 8° min⁻¹. The FTIR spectrum was recorded on a TENSOR II FTIR spectrophotometer (Bruker, Billerica, MA, USA). The hydrotalcite-like samples were pressed into KBr pellets. TG coupled with MS analysis was employed to analyze the thermal decomposition of the NiFe-LDH precursor. A Mettler Toledo 851[®] thermobalance system (Balzers Ltd., Milton Keynes, UK) was used for TG measurements, which were carried out in a flow of Ar (80 mL min⁻¹) for a temperature range of 25–800 °C with a heating rate of 10 K min⁻¹. A ThermoStar Balzers MS (Balzers Ltd., Milton Keynes, UK) was used to monitor the evolved gases during the thermal decomposition process. The textural structures of the NiFe-LDO catalysts were determined using an ASAP 2460 automated gas sorption (Micromeritics, Norcross, GA, USA) analyzer through the N₂ adsorption-desorption equilibrium at -196 °C. The specific surface area and pore diameter were determined and calculated by the Brunauer–Emmett–Teller (BET) and Barrett–Joyner–Halenda (BJH) methods, respectively. H₂-TPR and NH₃-TPD were performed on a TP-5080 instrument (Xianquan Industry and Trade Development Co. Ltd, Tianjin, China) coupled with MS using 0.08 g catalysts. Prior to the H₂-TPR test, the sample was pre-treated at 300 °C for 1 h in an Ar flow and then cooled to room temperature. Subsequently, the feeding gas was switched from Ar to 10% H₂/Ar (20 mL min⁻¹) and the temperature was increased from 30 °C to 900 °C with a heating rate of 10 K min⁻¹. In the case of NH₃-TPD, the samples were also pre-treated at 300 °C for 1 h, cooled to room temperature in a flow of He, and then saturated with 3% NH₃/He (25 mL min⁻¹) for 1 h at 50 °C. After NH₃ exposure, the sample was purged with He until excessive NH₃ was removed. Then, the TPD data were collected from 30 °C to 900 °C at a rate of 10 K min⁻¹ in He flow. XPS were recorded on a Thermo ESCALAB 250XI electron spectrometer (Thermo Fisher Scientific, Waltham, MA, USA) with Al K α as a radiation source (1486.6 eV). Binding energies of Ni 2p and Fe 2p were calibrated based on the graphite C 1s core level at 284.8 eV.

3.3. Catalytic Performance Tests

The NH₃-SCR activities over the catalysts were evaluated in a fixed-bed reactor with 0.38 g catalysts (40–60 mesh). The feed gas consisted of 600 ppm NO, 600 ppm NH₃, 5.0% O₂, 0 or 10.0% H₂O, 0 or 100 ppm SO₂, and balanced with N₂ at a flow rate of 350 cm³ min⁻¹, and the gas hourly space velocity (GHSV) was 45,000 h⁻¹. The inlet and outlet gas concentrations of NO, N₂O, NO₂, and NH₃ were detected by an online Fourier-transform-IR spectrometer (MultiGas[™] 6030) (MKS, Andover, MA, USA). The SCR reaction was carried out in the temperature range of 150–450 °C and the

data were recorded when the steady-state reaction was maintained after 30 min at each temperature. The NO_x conversion and N₂ selectivity were calculated according to the following expression:

$$\text{NO}_x \text{ conversion}(\%) = \frac{[\text{NO}]_{\text{in}} - [\text{NO}]_{\text{out}}}{[\text{NO}]_{\text{in}}} \times 100\%$$

$$\text{N}_2 \text{ selectivity}(\%) = \frac{[\text{NO}]_{\text{in}} + [\text{NH}_3]_{\text{in}} - [\text{NO}_2]_{\text{out}} - 2[\text{N}_2\text{O}]_{\text{out}}}{[\text{NO}]_{\text{in}} + [\text{NH}_3]_{\text{in}}} \times 100\%$$

where [NO]_{in} and [NH₃]_{in} refer to the inlet concentrations of NO and NH₃, respectively, and [NO]_{out}, [NO₂]_{out}, and [N₂O]_{out} refer to the reactor outlet concentrations of NO, NO₂, and N₂O, respectively.

4. Conclusions

A series of NiFe mixed oxides catalysts derived from hydrotalcite-like precursors were prepared and novelly employed as NH₃-SCR catalysts. The result proposed that the ideal phase composition of NiFe mixed oxides catalysts was available via adjusting the calcination temperature of NiFe-LDH, which had a significant effect on DeNO_x activity. The oxide phase formed at a lower calcination temperature is propitious for a better redox property and low-temperature activity, while the presence of NiFe₂O₄ spinels could contribute to high-temperature activity as well as SO₂ resistance and stability. We testify to NiFe-500 being the optimal catalyst incorporating NiO and NiFe₂O₄ spinels, where the virtues of the two phases were synergistically exerted and the best NH₃-SCR performance was achieved.

Author Contributions: X.W. and Y.D. designed and administered the experiments. C.Z. and X.L. performed experiments. R.W. collected and analyzed data. R.W., X.W., and Y. D wrote the manuscript.

Acknowledgments: The project was supported by National Natural Science Foundation of China (No. 21073131), Shanxi Provincial (No. 201601D10207).

Conflicts of Interest: The authors declare no conflicts of interest.

References

- Gao, F.; Tang, X.; Yi, H.; Zhao, S.; Li, C.; Li, J.; Shi, R.; Meng, X. A review on selective catalytic reduction of NO_x by NH₃ over Mn-based catalysts at low temperatures: Catalysts, mechanisms, kinetics and DFT calculations. *Catalysts* **2017**, *7*, 199. [[CrossRef](#)]
- Liu, F.; Shan, W.; Lian, Z.; Liu, J.; He, H. The smart surface modification of Fe₂O₃ by WO_x for significantly promoting the selective catalytic reduction of NO_x with NH₃. *Appl. Catal. B Environ.* **2018**, *230*, 165–176. [[CrossRef](#)]
- Wang, W.; McCool, G.; Kapur, N.; Yuan, G.; Shan, B.; Nguyen, M.; Graham, U.M.; Davis, B.H.; Jacobs, G.; Cho, K.; Hao, X. Mixed-phase oxide catalyst based on Mn-mullite (Sm, Gd) Mn₂O₅ for NO oxidation in diesel exhaust. *Science* **2012**, *337*, 832–835. [[CrossRef](#)] [[PubMed](#)]
- Boningari, T.; Smirniotis, P.G. Impact of nitrogen oxides on the environment and human health: Mn-based materials for the NO_x abatement. *Curr. Opin. Chem. Eng.* **2016**, *13*, 133–141. [[CrossRef](#)]
- Zong, L.; Zhang, G.; Zhao, J.; Dong, F.; Zhang, J.; Tang, Z. Morphology-controlled synthesis of 3D flower-like TiO₂ and the superior performance for selective catalytic reduction of NO_x with NH₃. *Chem. Eng. J.* **2018**, *343*, 500–511. [[CrossRef](#)]
- Zhang, K.; Yu, F.; Zhu, M.; Dan, J.; Wang, X.; Zhang, J. Enhanced low temperature no reduction performance via MnO_x-Fe₂O₃/vermiculite monolithic honeycomb catalysts. *Catalysts* **2018**, *8*, 100. [[CrossRef](#)]
- Rizzotto, V.; Chen, P.; Simon, U. Mobility of NH₃-solvated cull ions in Cu-SSZ-13 and Cu-ZSM-5 NH₃-SCR catalysts: A comparative impedance spectroscopy study. *Catalysts* **2018**, *8*, 162. [[CrossRef](#)]
- Pappas, D.K.; Boningari, T.; Boolchand, P.; Smirniotis, P.G. Novel manganese oxide confined interweaved titania nanotubes for the low-temperature selective catalytic reduction (SCR) of NO_x, by NH₃. *J. Catal.* **2016**, *334*, 1–13. [[CrossRef](#)]

9. Liu, F.; He, H. Structure-activity relationship of iron titanate catalysts in the selective catalytic reduction of NO_x with NH₃. *J. Phys. Chem. C* **2010**, *114*, 16929–16936. [[CrossRef](#)]
10. Liu, C.; Yang, S.; Ma, L.; Peng, Y.; Hamidreza, A. Comparison on the performance of α-Fe₂O₃ and γ-Fe₂O₃ for selective catalytic reduction of nitrogen oxides with ammonia. *Catal. Lett.* **2013**, *143*, 697–704. [[CrossRef](#)]
11. Liu, F.; He, H.; Zhang, C.; Feng, Z.; Zheng, L.; Xie, Y.; Hu, T. Selective catalytic reduction of NO with NH₃ over iron titanate catalyst: Catalytic performance and characterization. *Appl. Catal. B Environ.* **2010**, *96*, 408–420. [[CrossRef](#)]
12. Yang, S.; Li, J.; Wang, C.; Chen, J.; Ma, L.; Chang, H.; Yan, N. Fe-Ti spinel for the selective catalytic reduction of NO with NH₃: Mechanism and structure–activity relationship. *Appl. Catal. B Environ.* **2012**, *117*, 73–80. [[CrossRef](#)]
13. Chen, Z.; Wang, F.; Li, H.; Yang, Q.; Wang, L.; Li, X. Low-temperature selective catalytic reduction of NO_x with NH₃ over Fe–Mn mixed-oxide catalysts containing Fe₃Mn₃O₈ phase. *Ind. Eng. Chem. Res.* **2012**, *51*, 202–212. [[CrossRef](#)]
14. Pena, D.A.; Uphade, B.S.; Smirniotis, P.G. TiO₂-supported metal oxide catalysts for low-temperature selective catalytic reduction of NO with NH₃: I. Evaluation and characterization of first row transition metals. *J. Catal.* **2004**, *221*, 421–431. [[CrossRef](#)]
15. Liu, Z.; Liu, H.; Feng, X.; Ma, L.; Cao, X.; Wang, B. Ni–Ce–Ti as a superior catalyst for the selective catalytic reduction of NO_x with NH₃. *Mol. Catal.* **2018**, *445*, 179–186. [[CrossRef](#)]
16. Thirupathi, B.; Smirniotis, P.G. Nickel-doped Mn/TiO₂ as an efficient catalyst for the low-temperature SCR of NO with NH₃: Catalytic evaluation and characterizations. *J. Catal.* **2012**, *288*, 74–83. [[CrossRef](#)]
17. Ueda, K.; Ang, C.A.; Ito, Y.; Ohyama, J.; Satsuma, A. NiFe₂O₄ as an active component of platinum-group metal free automotive three-way catalyst. *Catal. Sci. Technol.* **2016**, *6*, 5797–5800. [[CrossRef](#)]
18. Chen, L.; Niu, X.; Li, Z.; Dong, Y.; Zhang, Z.; Yuan, F.; Zhu, Y. Promoting catalytic performances of Ni–Mn spinel for NH₃-SCR by treatment with SO₂ and H₂O. *Chem. Commun.* **2016**, *85*, 48–51. [[CrossRef](#)]
19. Thirupathi, B.; Smirniotis, P.G. Effect of nickel as dopant in Mn/TiO₂, catalysts for the low-temperature selective reduction of NO with NH₃. *Catal. Lett.* **2011**, *141*, 1399–1404. [[CrossRef](#)]
20. Deling, Y.; Xinyong, L.; Qidong, Z. Preparation and characterization of Ni–Ti–O mixed oxide for selective catalytic reduction of NO under lean-burn conditions. *Chin. J. Catal.* **2013**, *34*, 1449–1455.
21. Chmielarz, L.; Rutkowska, M.; Kuśtrowski, P.; Drozdek, M.; Piwowarska, Z.; Dudek, B.; Michalik, M. An influence of thermal treatment conditions of hydrotalcite-like materials on their catalytic activity in the process of N₂O decomposition. *J. Therm. Anal. Calorim.* **2011**, *105*, 161–170. [[CrossRef](#)]
22. Tang, X.; Hao, J.; Xu, W.; Li, J. Low temperature selective catalytic reduction of NO_x with NH₃ over amorphous MnO_x catalysts prepared by three methods. *Chem. Commun.* **2007**, *8*, 329–334. [[CrossRef](#)]
23. Yan, Q.; Chen, S.; Qiu, L.; Gao, Y.; O'Hare, D.; Wang, Q. The synthesis of Cu_yMn_zAl_{1-z}O_x mixed oxide as a low-temperature NH₃-SCR catalyst with enhanced catalytic performance. *Dalton Trans.* **2018**, *47*, 2992–3004. [[CrossRef](#)] [[PubMed](#)]
24. Wu, X.; Ci, C.; Du, Y.; Liu, X.; Li, X.; Xie, X. Facile synthesis of NiAl-LDHs with tunable establishment of acid-base activity sites. *Mater. Chem. Phys.* **2018**, *211*, 72–78. [[CrossRef](#)]
25. Yan, Q.; Nie, Y.; Yang, R.; Cui, Y.; O'Hare, D.; Wang, Q. Highly dispersed Cu_yAlO_x, mixed oxides as superior low-temperature alkali metal and SO₂ resistant NH₃-SCR catalysts. *Appl. Catal. A Gen.* **2017**, *538*, 37–50. [[CrossRef](#)]
26. Zhang, P.; Qian, G.; Xu, Z.; Shi, H.; Ruan, X.; Yang, J.; Frost, R. Effective adsorption of sodium dodecylsulfate (SDS) by hydrocalumite (CaAl-LDH-Cl) induced by self-dissolution and re-precipitation mechanism. *J. Colloid Interface Sci.* **2012**, *367*, 264–271. [[CrossRef](#)] [[PubMed](#)]
27. Chmielarz, L.; Kuśtrowski, P.; Rafalska-Łasocho, A.; Dziembaj, R. Influence of Cu, Co and Ni cations incorporated in brucite-type layers on thermal behaviour of hydrotalcites and reducibility of the derived mixed oxide systems. *Thermochim. Acta* **2002**, *395*, 225–236. [[CrossRef](#)]
28. Ballarini, N.; Cavani, F.; Passeri, S.; Pesaresi, L.; Lee, A.F.; Wilson, K. Phenol methylation over nanoparticulate CoFe₂O₄ inverse spinel catalysts: The effect of morphology on catalytic performance. *Appl. Catal. A Gen.* **2009**, *366*, 184–192. [[CrossRef](#)]
29. Yan, K.; Wu, X.; An, X.; Xie, X. Facile synthesis and catalytic property of spinel ferrites by a template method. *J. Alloy. Compd.* **2013**, *552*, 405–408. [[CrossRef](#)]

30. Chin, S.; Park, E.; Kim, M.; Jeong, J.; Bae, G.N.; Jurng, J. Preparation of TiO₂ ultrafine nanopowder with large surface area and its photocatalytic activity for gaseous nitrogen oxides. *Powder Technol.* **2011**, *206*, 306–311. [[CrossRef](#)]
31. Zhao, K.; Han, W.; Tang, Z.; Lu, J.; Hu, X. High-Efficiency Environmental-Friendly Fe-W-Ti Catalyst for Selective Catalytic Reduction of NO with NH₃: The Structure–Activity Relationship. *Catal. Surv. Asia* **2018**, *22*, 20–30. [[CrossRef](#)]
32. Zhang, Q.; Liu, X.; Ning, P.; Song, Z.; Li, H.; Gu, J. Enhanced performance in NO_x reduction by NH₃ over a mesoporous Ce-Ti-MoO_x catalyst stabilized by a carbon template. *Catal. Sci. Technol.* **2015**, *5*, 2260–2269. [[CrossRef](#)]
33. Chen, L.; Li, R.; Li, Z.; Yuan, F.; Niu, X.; Zhu, Y. Effect of Ni doping in Ni_xMn_{1-x}Ti₁₀ (x = 0.1–0.5) on activity and SO₂ resistance for NH₃-SCR of NO studied with in situ DRIFTS. *Catal. Sci. Technol.* **2017**, *7*, 3243–3257. [[CrossRef](#)]
34. Xu, H.; Wang, Y.; Cao, Y.; Fang, Z.; Lin, T.; Gong, M.; Chen, Y. Catalytic performance of acidic zirconium-based composite oxides monolithic catalyst on selective catalytic reduction of NO_x with NH₃. *Chem. Eng. J.* **2014**, *240*, 62–73. [[CrossRef](#)]
35. Chang, H.; Li, J.; Su, W.; Shao, Y.; Hao, J. A novel mechanism for poisoning of metal oxide SCR catalysts: Base-acid explanation correlated with redox properties. *Chem. Commun.* **2014**, *50*, 10031–10034. [[CrossRef](#)] [[PubMed](#)]
36. Zhao, K.; Meng, J.; Lu, J.; He, Y.; Huang, H.; Tang, Z.; Zhen, X. Sol-gel one-pot synthesis of efficient and environmentally friendly iron-based catalysts for NH₃-SCR. *Appl. Sur. Sci.* **2018**, *445*, 454–461. [[CrossRef](#)]
37. Wang, H.; Qu, Z.; Dong, S.; Tang, C. Mechanism study of FeW mixed oxides to the selective catalytic reduction of NO_x with NH₃: In situ DRIFTS and MS. *Catal. Today* **2018**, *307*, 35–40. [[CrossRef](#)]
38. Li, X.; Li, K.; Peng, Y.; Li, X.; Zhang, Y.; Wang, D.; Li, J. Interaction of phosphorus with a FeTiO_x catalyst for selective catalytic reduction of NO_x with NH₃: Influence on surface acidity and SCR mechanism. *Chem. Eng. J.* **2018**, *347*, 173–183. [[CrossRef](#)]
39. Jiang, J.; Pan, H.; Sun, G.; Ye, Q.; Shao, Z.; Shi, Y. Promotion of Ni/H-BEA by Fe for NO_x Reduction with Propane in a Lean-Burn Condition. *Energ. Fuel* **2011**, *25*, 4377–4383. [[CrossRef](#)]
40. Sun, C.; Liu, H.; Chen, W.; Chen, D.; Yu, S.; Liu, A.; Dong, L.; Feng, S. Insights into the Sm/Zr co-doping effects on N₂ selectivity and SO₂ resistance of a MnO_x-TiO₂ catalyst for the NH₃-SCR reaction. *Chem. Eng. J.* **2018**, *347*, 27–40. [[CrossRef](#)]
41. Tiwari, S.; Prakash, R.; Choudhary, R.J.; Phase, D.M. Oriented growth of Fe₃O₄ thin film on crystalline and amorphous substrates by pulsed laser deposition. *J. Phys. D Appl. Phys.* **2007**, *40*, 4943. [[CrossRef](#)]
42. Wan, Y.; Zhao, W.; Tang, Y.; Li, L.; Wang, H.; Cui, Y.; Shi, J. Ni-Mn bi-metal oxide catalysts for the low temperature SCR removal of NO with NH₃. *Appl. Catal. B Environ.* **2014**, *148*, 114–122. [[CrossRef](#)]
43. Kang, M.; Park, E.D.; Kim, J.M.; Yie, J.E. Cu-Mn mixed oxides for low temperature NO reduction with NH₃. *Catal. Today* **2006**, *111*, 236–241. [[CrossRef](#)]
44. Ogawa, M.; Asai, S. Hydrothermal synthesis of layered double hydroxide-deoxycholate intercalation compounds. *Chem. Mater.* **2000**, *12*, 3253–3255. [[CrossRef](#)]

